BIOCHEMISTRY
including biophysical chemistry & molecular biology

Article

pubs.acs.org/biochemistry

A Compact Intermediate State of Calmodulin in the Process of Target Binding

Yoshiteru Yamada,*[,†] Tatsuhito Matsuo,[†,‡,§] Hiroyuki Iwamoto,[†] and Naoto Yagi[†,‡]

[†]SPring-8, Japan Synchrotron Radiation Research Institute, Kouto, Sayo, Hyogo 679-5198, Japan

[‡]Core Research for Evolutional Science and Technology, Japan Science and Technology Agency, Saitama, Japan

Supporting Information

ABSTRACT: Calmodulin undergoes characteristic conformational changes by binding Ca^{2+}, which allows it to bind to more than 300 target proteins and regulate numerous intracellular processes in all eukaryotic cells. We measured the conformational changes of calmodulin upon Ca^{2+} and mastoparan binding using the time-resolved small-angle X-ray scattering technique combined with flash photolysis of caged calcium. This measurement system covers the time range of 0.5−180 ms. Within 10 ms of the stepwise increase in Ca^{2+} concentration, we identified a distinct compact conformational state with a drastically different molecular dimension. This process is too fast to study with a conventional stopped-flow apparatus. The compact conformational state was also observed without mastoparan, indicating that the calmodulin forms a compact globular conformation by itself upon Ca^{2+} binding. This new conformational state of calmodulin seems to regulate Ca^{2+} binding and conformational changes in the N-terminal domain. On the basis of this finding, an allosteric mechanism, which may have implications in intracellular signal transduction, is proposed.

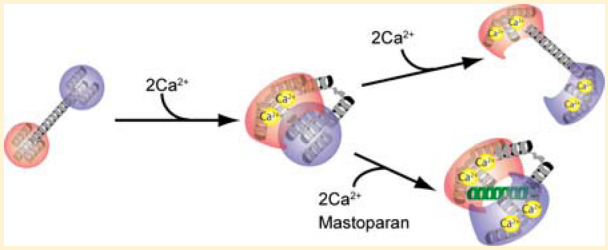

Calmodulin (CaM) is a small Ca^{2+}-binding protein that exists in all eukaryotic cells. CaM plays essential roles in Ca^{2+} signaling, regulating numerous intracellular processes such as cell growth, proliferation, motility, and apoptosis. It has four helix−loop−helix calcium binding motifs commonly called EF-hand motifs. Two EF-hand motifs form a globular domain, and the globular domains at the N- and C-termini are connected by a flexible linker helix. Without Ca^{2+}, CaM assumes an extended dumbbell structure.[1] The conformation of EF-hand motifs in each globular domain is antiparallel, and the hydrophobic residues are buried inside the protein. Binding of Ca^{2+} to the two EF-hands in each globular domain alters the interhelical angle in the EF-hand motifs, causing a structural change in the domain from "closed" to "open".[1,2] In this open conformation, the helix that connects the two domains is dynamically disordered and the two domains are flexible.[3−7] It has been reported that in this conformation hydrophobic residues, especially Met, become exposed to the solvent, facilitating binding of CaM to a large number of target molecules.[8] When binding a target molecule, CaM assumes a more compact structure.[3,9]

The kinetics of Ca^{2+}-induced CaM activation, which has a direct implication in Ca^{2+} signaling, has not been resolved. Recently, Park et al. investigated the kinetics of CaM conformational changes upon Ca^{2+} binding using acrylodan fluorescence in a microfluidic mixer.[10] They found that the kinetic rates of the conformational changes in the two globular domains differ by more than 1 order of magnitude. The characteristic time constants are ∼490 μs for the transition in the C-terminal domain and ∼20 ms for that in the N-terminal domain. However, the previous studies revealed only local conformational changes because the measurement relied on site sensitive methods such as fluorescence spectroscopy coupled with site-directed mutagenesis or modification. Although information about the local structure is important, changes in the dimension and shape of a protein molecule during conformational changes are also crucial for understanding the mechanism of protein dynamics and expression of protein function. The stopped-flow small-angle X-ray scattering (SAXS) technique using synchrotron radiation is very effective for monitoring changes in the overall shape of proteins.[11] However, characterization of a protein in solution using SAXS requires a high-precision SAXS profile, which has been difficult to obtain at a time resolution that matches the fast kinetics of protein conformational changes, mainly because of the insufficient X-ray flux and the low protein concentration. Recently, fast solution scattering measurements at low protein concentration have become possible by using high-brilliance X-ray beams from synchrotron radiation. Here, we have investigated the kinetics of Ca^{2+}-induced structural change of CaM using the new time-resolved SAXS technique.

In this study, the kinetics of Ca^{2+} binding and subsequent conformational changes was triggered by the release of Ca^{2+} from a caged Ca^{2+} chelator, DM-nitrophen.[12] DM-nitrophen binds Ca^{2+} with high affinity. Upon exposure of the DM-nitrophen−Ca^{2+} complex to near-UV light, the chelator is

Received: February 17, 2012
Revised: April 9, 2012
Published: May 1, 2012

   dx.doi.org/10.1021/bi3002192 | *Biochemistry* 2012, 51, 3963−3970

cleaved yielding an iminodiacetic product with a much lower affinity for Ca^{2+} and causes an increase in the free Ca^{2+} concentration. Furthermore, the rate of release of Ca^{2+} of DM-nitrophen upon illumination is $\sim 3.8 \times 10^4$ s^{-1},[13] so that it would not become a rate-limiting step during the measurement of the kinetics of CaM. The Ca^{2+} binding and subsequent conformational changes were investigated by the continuous SAXS measurement coupled with flash photolysis. Within the time scale of 0.5−180 ms, we identified a distinct new compact conformational state with a drastically different molecular dimension that is formed before Ca^{2+} binds to the N-terminal domain and CaM binds to the target peptide.

MATERIALS AND METHODS

Calmodulin from bovine brain and DM-nitrophen were purchased from Wako Jun'yaku and Invitrogen, respectively. Mastoparan, which is used as a model peptide for a target protein of CaM, was purchased from Peptide Institute, Inc. (Osaka, Japan). Other chemicals were of analytical grade.

CaM was solubilized in a buffer solution containing 50 mM Tris-HCl (pH 7.5), 100 mM NaCl, 1.11 mM DM-nitrophen, and 1.11 mM $CaCl_2$. The protein concentration was 1.25 mg/mL (0.075 mM), which was spectrophotometrically measured in the stock solution without DM-nitrophen using the extinction coefficient at 280 nm that was calculated from the amino acid sequence[14] (ε_{280} = 2980 cm^{-1} M^{-1}).

The SAXS measurement was performed on beamline BL40XU at SPring-8.[15] The X-ray wavelength was 0.1 nm, and the sample-to-detector distance was 1700 mm. The X-ray flux was $\sim 7 \times 10^{14}$ photons/s. The X-ray scattering was recorded with an X-ray image intensifier (V5445P, Hamamatsu Photonics, Hamamatsu, Japan) coupled to a high-speed CMOS camera (FASTCAM SA 1.1, Photron) with 1024 × 1024 pixels. The beam center and the exact sample-to-detector distance were determined by measurement of a powder diffraction pattern of silver behenate (d = 5.838 nm).[16]

The technical details of the laser flash photolysis system have been described previously.[17] The optical cell was designed so that the simultaneous exposure to an X-ray beam and a Nd:YAG pulse laser beam was permitted. The cell had two windows for the X-ray beam and a window for the laser beam, which were all made of thin (<0.05 mm) quartz. The optical paths of the two beams were oriented at 90° with respect to each other. The path lengths for both X-rays and laser light were 1.5 mm. The transmittance of Nd:YAG pulse laser light was ∼70−80% at 1.0 mm, as estimated from the absorption coefficient of DM-nitrophen (ε_{355} = 2500 cm^{-1} M^{-1}). The rate of release of Ca^{2+} from DM-nitrophen is $\sim 3.8 \times 10^4$ s^{-1},[13] which is faster than the time resolution of our time-resolved SAXS measurement (0.5 ms). The concentration of the released Ca^{2+} was 345 μM ($[Ca^{2+}]/[CaM]$ = 4.6), which was measured by fluo-3 (Invitrogen) fluorescence using a fluorescence spectrophotometer (F-2500, Hitachi High-tech).

SAXS data collection was performed during the descent of the sample stage at a speed of 50 mm/s. Thirty milliseconds after the measurement of SAXS profiles had begun, flash photolysis was performed by illumination with 355 nm light from a high-power Nd:YAG pulse laser (SureliteII-10, Continuum), and the time-resolved SAXS profiles were collected every 0.5 ms for 180 ms.

The two-dimensional scattering patterns were radially integrated using Fit2D[18] to obtain a one-dimensional data set corresponding to the scattering profile. The solvent scatter (background scatter) was obtained by measuring scatter from 50 mM Tris-HCl (pH 7.5), 100 mM NaCl, 1.11 mM DM-nitrophen, 1.11 mM $CaCl_2$, and 0.074 mM mastoparan. The solvent scatter was averaged over 100 data sets. The averaged solvent scattering profile was then subtracted from each scattering profile of CaM.

To estimate the forward scattering intensity and the radius of gyration, we analyzed all scattering curves with the Guinier approximation. The small-angle region of scattering curve was approximated by

$$I(Q) = I(0) \exp(-Q^2 R_g^{\ 2}/3)$$

where $I(0)$ is the forward scattering intensity at a zero angle. Q is defined as $Q = 4\pi \sin(2\theta/2)/\lambda$, where 2θ is the scattering angle and λ is the wavelength of the X-ray (0.1 nm). The radius of gyration, R_g, and forward scattering intensity, $I(0)$, were estimated in the Guinier region ($QR_g < 1.3$).[19,20] Background subtraction, averaging, and Guinier approximation were performed semiautomatically using a homemade macro in IGOR Pro (WaveMatrics, Inc.). To correct for the scattering intensity changes due to variation in the path length (which is caused by nonuniform separation between two windows of the sample cell), the change in the $I(0)$ value in the time-resolved measurement was normalized by the change in the total integrated intensity of lysozyme scatter measured in the same manner. The correction factor was 20% at maximum. The data points from 0 to 150 ms after flash photolysis were used. Kinetic curves were also analyzed using IGOR Pro with a three-state sequential model. The $R_g^{\ 2}$ and $I(0)$ values at zero and infinite time were assumed to be those obtained in static measurements in the absence or presence of mastoparan and 3 mM $CaCl_2$, respectively. The statistics are given as means and the standard deviation.

RESULTS

Conformation of Calmodulin in Equilibrium. Figure 1 shows Ca^{2+}-induced R_g changes of CaM with or without mastoparan measured under equilibrium conditions. The R_g value of Ca^{2+}-free CaM without mastoparan (apo-CaM) was 20.4 ± 0.2 Å. Upon an addition of 2 mol of Ca^{2+}/mol of CaM, R_g increased to 21.6 ± 0.3 Å (mean ± standard deviation) [Figure 1A (●)]. The R_g values estimated with Crysol[21] from the NMR structure of apo-CaM [Protein Data Bank (PDB) entry 1CFD][1] and Ca^{2+}-saturated CaM without a target peptide (Ca_4-CaM, PDB entry 1CLL)[22] were 20.3 and 21.9 Å, respectively. Thus, the R_g values of CaM in the presence and absence of Ca^{2+} ions were similar to the expected R_g values. It is known that binding of Ca^{2+} leads to substantial alteration of the interhelical angles within the EF-hands in each domain and induces the open conformation.[2,23] In fact, the $I(0)$ values seem to be independent of the Ca^{2+} concentration, indicating that the molecular mass was unchanged upon binding of Ca^{2+} to the N- and C-terminal domains [Figure 1B (●)]. Therefore, the small Ca^{2+}-induced increase in R_g of CaM without mastoparan indicates conformational changes of the N- and C-terminal domains that cause a transition from a closed to open structure.[24]

In the presence of mastoparan, however, the Ca^{2+}-induced changes in R_g and $I(0)$ of CaM were different from those without mastoparan (Figure 1A,B). The R_g value of CaM decreased in the presence of Ca^{2+}, reaching 18.7 ± 0.4 Å with 2−3 mol of Ca^{2+}/mol of CaM [Figure 1A (○)]. These results

dx.doi.org/10.1021/bi3002192 | Biochemistry 2012, 51, 3963−3970

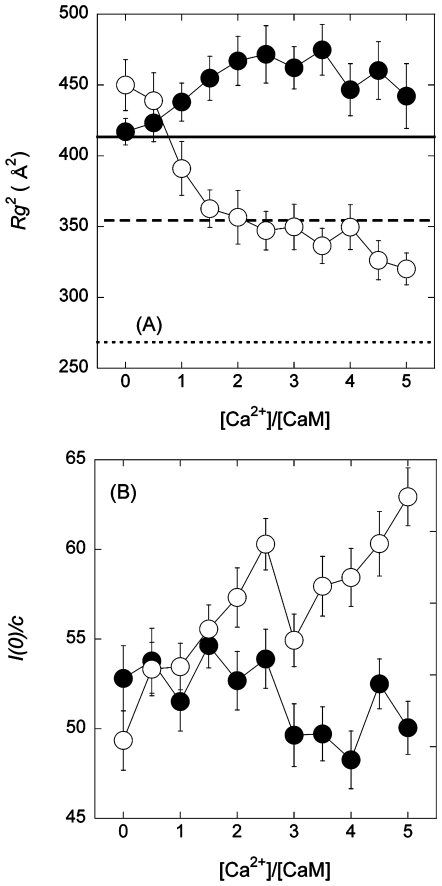

Figure 1. Changes in R_g (A) and $I(0)/c$ (B) of CaM due to Ca^{2+} binding with (○) and without (●) mastoparan. In panel A, the solid, dashed, and dotted lines show the R_g^2 values at −5, 10, and 140 ms, respectively, in the time-resolved experiments with mastoparan (Figure 2B). The error bars represent the standard deviation of three measurements.

indicate that, in the presence of mastoparan, CaM assumes a compact globular conformation with Ca^{2+}, as reported in the previous studies.[25,26] The increase in the $I(0)$ value of CaM with mastoparan (Figure 1B) indicates an increase in its molecular mass of ∼1.5 kDa, which is close to the molecular mass of mastoparan calculated from its amino acid sequence (1.479 kDa). For both R_g and $I(0)$, the changes were complete upon addition of ∼2−3 mol of Ca^{2+}/mol of CaM.

Conformational Changes of Calmodulin upon Ca^{2+} Binding. The conformational change of CaM was monitored by R_g and $I(0)$ estimated via Guinier approximation of a SAXS profile in each frame (Figure 2). To confirm the R_g^2 and $I(0)$ values under the initial and final conditions of the time-resolved SAXS measurement, we measured the SAXS profiles in the steady states (Figure 2A). Using the experimental setup for the time-resolved experiment and a laser flash, the scatter was measured from the sample solution in the absence and presence of mastoparan with an excess concentration of Ca^{2+} (∼3 mM). The steady-state SAXS scatter had constant R_g^2 and $I(0)$ values that corresponded to the final states of the kinetics measurements (Figure 2A).

Release of Ca^{2+} from the caged compound caused significant changes in R_g^2 and $I(0)$ with and without mastoparan (Figure 2B,C). Before flash photolysis, the R_g was 20.4 ± 0.5 Å in the presence and absence of mastoparan, which was close to the R_g in the absence of Ca^{2+} (Figure 1A). To understand the dominant conformation of CaM, we compared the experimental scattering profile and the theoretical scattering profile calculated from crystal and NMR solution structures using Crysol.[21] The SAXS profile at −5 ms (before flash photolysis) was indistinguishable from the theoretical SAXS profile calculated from the NMR structure (PDB entry 1CFD)[1] (Figure 3 and Figure S1 and Table S1 of the Supporting Information). These results indicate that CaM assumes an expanded dumbbell-like conformation with closed N- and C-terminal domains before flash photolysis in the absence and presence of mastoparan.

In the presence of mastoparan, R_g^2 decreased drastically within 20 ms of photolysis (Figure 2B). The R_g value at 10 ms, ∼14 Å, was much smaller than that before photolysis. Furthermore, the Kratky plot at 10 ms has a clear peak at 0.1 Å^{-1}. If the conformational change was ascribed to binding of mastoparan to CaM, $I(0)$ should increase because of the larger molecular mass. However, $I(0)$ was unchanged within 20 ms [Figure 2C (●)]. The time-resolved SAXS profile without mastoparan also showed a drastic decrease in R_g^2 within 20 ms of photolysis, while $I(0)$ was unchanged. These results show that a compact intermediate transiently accumulates at the early stage of the Ca^{2+}-induced conformational change of CaM regardless of whether there is a target peptide around the CaM molecule. Because a similar decrease in R_g was observed with a reduced amount of Ca^{2+} (2.1 Ca^{2+}/CaM molar ratio) in the presence of mastoparan (Figure 2D), formation of the intermediate does not require full occupation of the four Ca sites in CaM.

The time-resolved SAXS results after 20 ms were different with and without mastoparan (Figure 2B,C). The R_g^2 of CaM with mastoparan slightly increased from 20 ms, while the R_g^2 of CaM without mastoparan increased much more and did not saturate at 140 ms (Figure 2B). $I(0)$ of CaM with mastoparan slightly increased from 20 ms and saturated at 140 ms (Figure 2C), indicating that the molecular mass increases with mastoparan binding. At 140 ms, the ratio of $I(0)$ in the presence and absence of mastoparan (1.14 times) was close to the molecular mass ratio between the apo-CaM and mastoparan-bound CaM (1.13 times). Furthermore, the SAXS profile at 140 ms showed a compact conformation with an R_g of 15.2 ± 0.2 Å. These results, together with the fact that the SAXS profile at 140 ms was indistinguishable from the theoretical SAXS profile of the solution structure of a CaM−target peptide complex (PDB entry 2BBM)[27] (Figure 3C,D and Table S1 of the Supporting Information), indicate that the conformational change of CaM from 20 ms onward can be ascribed to binding of mastoparan to Ca-bound CaM. When the amount of released Ca^{2+} was reduced, R_g^2 similarly stayed at a low level in the presence of mastoparan and $I(0)$ increased gradually (Figure 2D).

In Figure 2C, $I(0)$ of CaM without mastoparan did not change from 0 to 140 ms, while R_g^2 drastically increased after 20 ms (Figure 2B). Thirty seconds after the flash photolysis, the R_g^2 value showed that the molecular dimension of CaM was slightly larger than that before photolysis, while $I(0)$ was unchanged. These results, together with the fact that the SAXS profile at 30 s was indistinguishable from that estimated from the crystal structure of Ca_4-CaM without mastoparan (PDB entry 1CLL)[22] (Figure 3C,D and Table S1 of the Supporting Information), indicate that the slow kinetic phase of CaM without mastoparan can be ascribed to the process in which

dx.doi.org/10.1021/bi3002192 | Biochemistry 2012, 51, 3963−3970

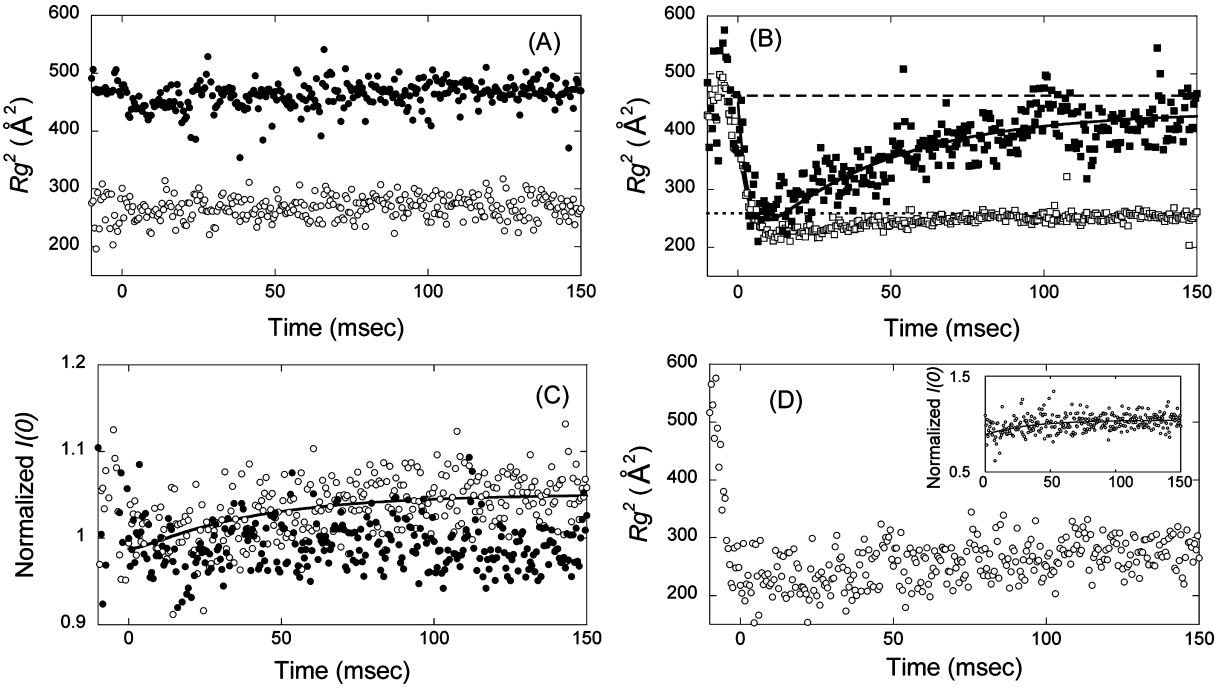

Figure 2. Results of time-resolved SAXS experiments for CaM with and without mastoparan. (A) R_g^2 in the presence (○) and absence (●) of mastoparan with an excess concentration of Ca^{2+} (~3 mM). (B) R_g^2 after the release of excess Ca^{2+}: (■) kinetics without mastoparan and (□) kinetics with mastoparan. The dotted and dashed lines show the average values with and without mastoparan, respectively. The solid line shows results of fitting with our model. (C) $I(0)$ after the release of excess Ca: (●) kinetics without mastoparan and (○) kinetics with mastoparan. The data were normalized by average $I(0)$ before Ca release. (D) R_g^2 after release of 2.2 mol of Ca^{2+}/mol of CaM in the presence of mastoparan. The inset shows $I(0)$. Each value was obtained by averaging R_g^2 and $I(0)$ in 25 or 15 runs in the experiments with or without mastoparan, respectively. The details of the statistics are given in Table S2 of the Supporting Information.

CaM assumes an expanded dumbbell-like structure with an open conformation at both N- and C-terminal domains.

Characterization of Kinetics of Ca^{2+} and Mastoparan Binding. Kinetics of R_g^2 and $I(0)$ of CaM with or without mastoparan seem to have a three-state transition (Figure 2). Therefore, we assume, as a simplest model, a three-state transition among an initial conformation (CaM_{init}), a compact globular intermediate (CaM_{int}), and a final conformation of CaM (CaM_{fin}). CaM_{fin} in the presence of mastoparan differs drastically from CaM_{fin} in the absence of mastoparan.

$$CaM_{init} \xrightarrow{k_a} CaM_{int} \xrightarrow{k_b} CaM_{fin}$$

where k_a and k_b are the rate constants between the conformational states. Although the kinetics of R_g^2 of CaM was approximated as a three-state process, the kinetics of $I(0)$ of CaM with mastoparan was assumed to be a two-state process between CaM_{int} and CaM_{fin} because mastoparan binding was observed only after the accumulation of CaM_{int} (Figure 2B,C). On the other hand, $I(0)$ of CaM without mastoparan remained constant (Figure 2C). Kinetics curves of both R_g^2 and $I(0)$ were well fitted with our model (Figure 2B,C). Table 1 shows the kinetic parameters of CaM with and without mastoparan.

R_g at time zero was estimated by extrapolation to be 18.7 ± 4.6 and 20.1 ± 4.7 Å with and without mastoparan, respectively. Although the differences are statistically insignificant, these R_g values were slightly smaller than that of apo-CaM [20.4 ± 0.2 Å (Figure 1)] and the observed R_g values before flash photolysis [21.1 ± 0.5 Å (Figure 2B)]. Although the amount of bound Ca^{2+} cannot be measured directly by SAXS, it is likely that binding of two Ca^{2+} ions to the C-terminal domain has taken place within the dead time of the present measurement because Park et al. found that the conformational change in the C-terminal domain occurs with a time constant of ~490 μs.[10] Therefore, CaM_{int} in our kinetic scheme actually represents Ca_2-CaM, and this study shows that the conformational change from Ca_2-CaM to CaM_{int} occurs with a τ of 3.74 ms. Because this process is unchanged when the amount of released Ca^{2+} was decreased (Figure 2D), it does not seem to require binding of further Ca^{2+} to the N-terminal domain. After CaM_{int} is formed, R_g^2 slightly increases with a k_b of 0.025 ms^{-1} (τ ~ 39.95 ms). This process involves binding of mastoparan, which is evident in the increase in $I(0)/I(Q)_{intg}$. It is not certain whether two additional Ca^{2+} ions bind to the N-terminal domain during this phase because the result at a lower Ca^{2+} concentration (Figure 2D, inset) was similar. In the absence of mastoparan, the fitting gave a k_b of 0.02 ms^{-1} with an asymptotic value of ~400 for R_g^2. The final state of Ca_4-CaM has an R_g^2 of ~470 Å that is even larger at 30 s.

■ DISCUSSION

We performed a fast time-resolved SAXS measurement of CaM with and without mastoparan coupled with the flash photolysis technique. Previously, the time-resolved SAXS measurement at fast kinetics has been difficult because characterization of protein structure in solution by SAXS requires a scattering profile with high precision. Our SAXS technique allows us to perform rapid kinetic studies at a protein concentration as low as 75 μM because of the highly brilliant X-ray beam and the flash photolysis technique. New kinetic results with regard to the conformational changes of CaM within 150 ms of Ca^{2+} binding were obtained.

dx.doi.org/10.1021/bi3002192 | Biochemistry 2012, 51, 3963−3970

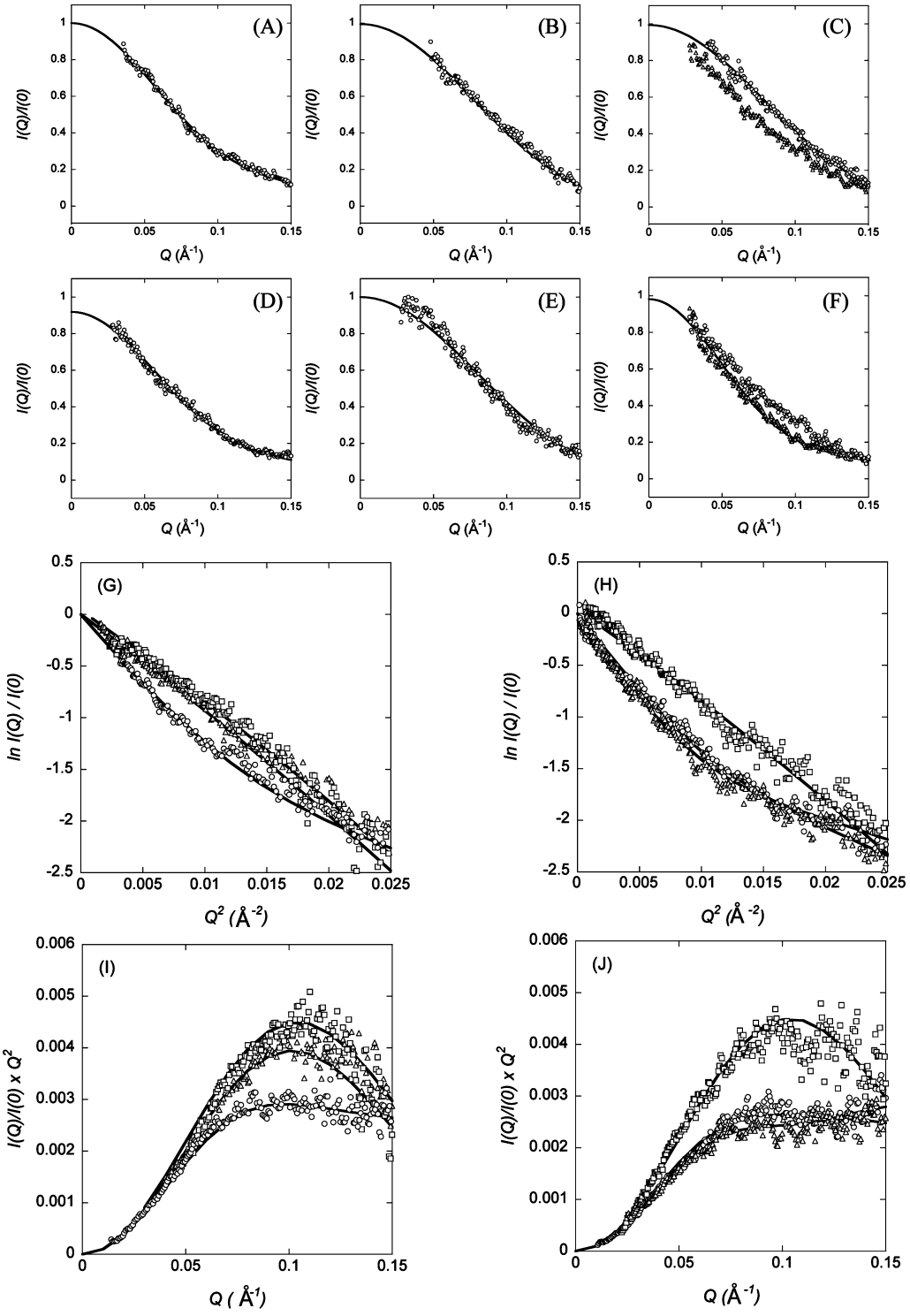

Figure 3. SAXS profiles of CaM in the presence (A–C) and absence (D–F) of mastoparan. Panels A–C represent the scattering profiles at 0.5, 10, and 140 ms, respectively. Panels D–F represent the same time points as panels A–C. In panels C and F, the triangles represent the scattering profile at 30 s. In panel C, the profile at 30 s does not fit the crystal structure (PDB entry 2BBM). In panel F, the profile at 140 ms does not fit the crystal structure (PDB entry 1CCL). Panels G and H and panels I and J represent the Guinier plot and Kratky plot, respectively, of CaM in the presence (G) and absence (H) of mastoparan. The circles, squares, diamonds, and triangles represent the scattering profiles at 0.5 ms, 10 ms, 140 ms, and 30 s, respectively. In all panels, the solid lines are the theoretical curves calculated from a crystal or NMR solution structure with Crysol: part of PDB entry 1K93 (for the Ca_2-CaM adenylyl cyclase complex)[31] for 0.5 ms (panels A, D, and G–I), PDB entry 1PRW (for a Ca_4-CaM compact structure)[28] for 10 ms (panels B, E, and G–J), PDB entry 2BBM (for a Ca_4-CaM–target peptide complex)[27] for 140 ms in the presence of mastoparan (panels C, G, and I), and PDB entry 1CLL (for a Ca_4-CaM complex without a target peptide)[22] for 30 s in the absence of mastoparan (panels F, H, and J). The χ values of the fit are listed in Table S1 of the Supporting Information.

We observed a new kinetic intermediate state within 10 ms of Ca^{2+} release, which has a smaller molecular dimension than Ca_4-CaM with mastoparan (Figure 4). This intermediate is characterized by its small molecular dimension and compact

dx.doi.org/10.1021/bi3002192 | *Biochemistry* 2012, 51, 3963–3970

Table 1. Kinetic Parameters Obtained by Data Fitting with a Three-State Model

			R_g (Å)			$I(0)$	
	k_a (ms^{-1})	k_b (ms^{-1})	CaM_{init}	CaM_{int}	CaM_{fin}	CaM_{int}	CaM_{fin}
CaM with mastoparan	0.267 ± 0.073	0.025 ± 0.008	18.7 ± 4.6	13.7 ± 3.4	15.2 ± 1.5	28.2 ± 0.4	30.8 ± 0.1
CaM without mastoparan	0.304 ± 0.062	0.023 ± 0.003	20.1 ± 4.7	13.4 ± 3.3	20.8 ± 2.5	28.4 ± 1.1	28.4 ± 1.0

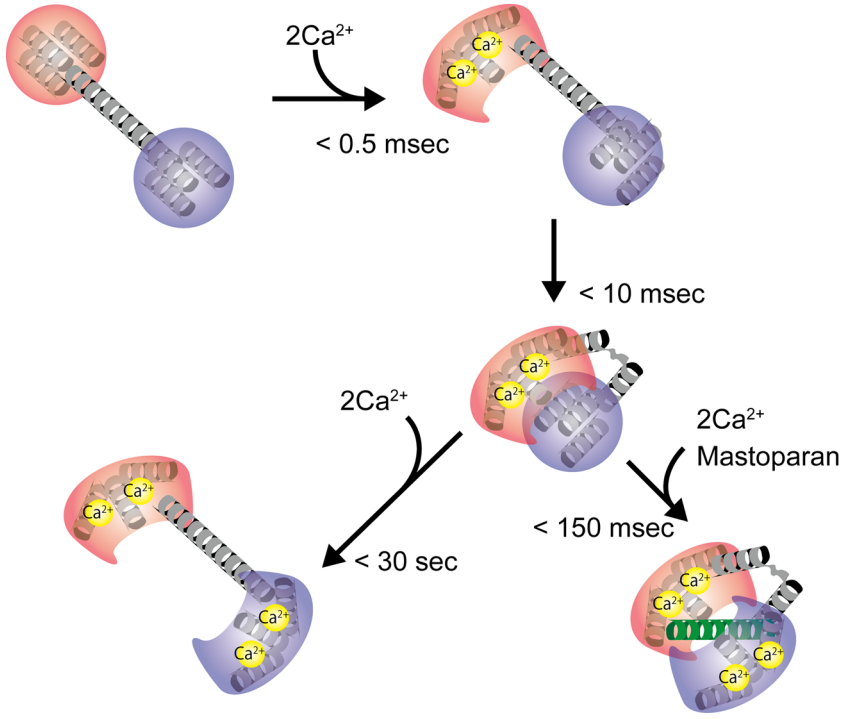

Figure 4. Schematic illustration of the kinetic reaction of CaM upon Ca^{2+} binding. The N- and C-terminal domains and Ca^{2+} ions are colored blue, red, and yellow, respectively. The green helix shows mastoparan. Helices in each domain are colored gray.

shape that are suggested by R_g and the shape of the Kratky plot (Figure 3). This state was also observed without mastoparan (Figure 2B), suggesting that CaM assumes a compact conformation by itself upon Ca^{2+} binding.

A compact globular structure of CaM without target protein or peptide has been determined by X-ray crystallography at pH 6.0 (PDB entry 1PRW).[28] The theoretical SAXS profile estimated from this structure with Crysol was similar to the SAXS profile 10 ms after photolysis (Figure 3), indicating that the global shape of the compact intermediate has the same characteristic features as the crystal structure of closed compact globular CaM. Studies with computer simulation and circular dichroism have also suggested that CaM without bound Ca^{2+} adopts a closed compact spherical structure at low ionic strengths (0.1 M KCl).[29] In this conformation, the hydrophobic pockets are shielded from the bulk solvent with the closed N-terminal domain buried in the open C-terminal domain.[28,29] These results suggest that, upon Ca binding, CaM initially assumes a Ca_2-CaM intermediate in which the hydrophobic sites are exposed to the bulk solvent. Then, CaM needs to transiently adopt a small compact intermediate state that is energetically more stable because the hydrophobic surface is buried. Mastoparan can stabilize this compact structure by entering between the two domains and covering the hydrophobic surfaces of the two domains (Figure 2B). This process corresponds to a conformational change in the N-terminal domain that takes ~20 ms.[10] Because other CaM-binding proteins also cause a globular conformation of CaM, this mechanism seems common among them.

The Ca^{2+} titration experiment at a $[Ca^{2+}]/[CaM]$ ratio of >2 (Figure 1A) indicated that CaM under an equilibrium condition assumes an expanded or compact conformation in the absence or presence of mastoparan, respectively. In the kinetic experiment in the absence of mastoparan, CaM returns to the expanded conformation after assuming the compact intermediate (Figure 2B). In the presence of mastoparan, R_g^2 under an equilibrium condition was larger than R_g^2 at 140 ms in the kinetic experiments. This is probably because at equilibrium there is more than one conformational state. On the other hand, most of the CaM molecules seem to adopt a compact conformation with mastoparan at 140 ms. This is demonstrated by the fact that the scattering profiles were similar to the theoretical scattering curve calculated from a crystal structure (Figures 2 and 3C and Table S1 of the Supporting Information).

These results show that CaM assumes a compact intermediate before binding a target peptide. This two-step mechanism may be important in intracellular signal transduction. It ensures that the signal is transmitted only when the increase in Ca^{2+} concentration is sufficiently long and large and avoids responding to a spurious rise in Ca^{2+} concentration. For example, a short (<20 ms), localized increase in the intracellular Ca^{2+} concentration has been reported in muscles, neurons, and other excitable and nonexcitable cells ("calcium sparks").[30] Cellular responses to such a short rise in Ca^{2+} concentration

dx.doi.org/10.1021/bi3002192 | Biochemistry 2012, 51, 3963−3970

may be suppressed by the two-step mechanism of CaM that is suggested in this study.

■ ASSOCIATED CONTENT

Supporting Information

Fitting parameters for each crystal or NMR solution structure using Crysol (Table S1) and averages and standard deviations associated with the data points presented in Figure 2 (Table S2). This material is available free of charge via the Internet at http://pubs.acs.org.

■ AUTHOR INFORMATION

Corresponding Author

*SPring-8, Japan Synchrotron Radiation Research Institute, 1-1-1 Kouto, Sayo-cho, Sayo-gun, Hyogo 679-5198, Japan. Phone: +81-791-58-2750. Fax: +81-791-58-0830. E-mail: teru@spring8.or.jp.

Present Address

[§]Quantum Beam Science Directorate, Japan Atomic Energy Agency, 2-4 Shirane Shirakata, Tokai-mura, Naka-gun, Ibaraki 319-1195, Japan.

Funding

This work was supported by CREST/JST.

Notes

The authors declare no competing financial interest.

■ ACKNOWLEDGMENTS

The experiment was conducted with the approval of the SPring-8 Program Review Committee (2009B1547, 2010B1454, 2010B2031, and 2011B2081).

■ ABBREVIATIONS

CaM, calmodulin; NMR, nuclear magnetic resonance; SAXS, small-angle X-ray scattering; R_g, radius of gyration; $I(0)$, forward X-ray scattering intensity; apo-CaM, calmodulin without Ca^{2+} or a target peptide; Ca_2-CaM, calmodulin bound to two Ca^{2+} ions; Ca_4-CaM, calmodulin bound to four Ca^{2+} ions; CaM_{init}, initial conformation of calmodulin; CaM_{int}, compact globular intermediate of calmodulin; CaM_{fin}, final conformation of calmodulin.

■ REFERENCES

(1) Kuboniwa, H., Tjandra, N., Grzesiek, S., Ren, H., Klee, C. B., and Bax, A. (1995) Solution structure of calcium-free calmodulin. *Nat. Struct. Biol. 2*, 768−776.

(2) Zhang, M., Tanaka, T., and Ikura, M. (1995) Calcium-induced conformational transition revealed by the solution structure of apo calmodulin. *Nat. Struct. Biol. 2*, 758−767.

(3) Baber, J. L., Szabo, A., and Tjandra, N. (2001) Analysis of slow interdomain motion of macromolecules using NMR relaxation data. *J. Am. Chem. Soc. 123*, 3953−3959.

(4) Bertini, I., Del Bianco, C., Gelis, I., Katsaros, N., Luchinat, C., Parigi, G., Peana, M., Provenzani, A., and Zoroddu, M. A. (2004) Experimentally exploring the conformational space sampled by domain reorientation in calmodulin. *Proc. Natl. Acad. Sci. U.S.A. 101*, 6841−6846.

(5) Zhang, M., Tanaka, T., and Ikura, M. (1995) Calcium-induced conformational transition revealed by the solution structure of apo calmodulin. *Nat. Struct. Biol. 2*, 758−767.

(6) Wang, T., Frederick, K. K., Igumenova, T. I., Wand, A. J., and Zuiderweg, E. R. (2005) Changes in calmodulin main-chain dynamics upon ligand binding revealed by cross-correlated NMR relaxation measurements. *J. Am. Chem. Soc. 127*, 828−829.

(7) Barbato, G., Ikura, M., Kay, L. E., Pastor, R. W., and Bax, A. (1992) Backbone dynamics of calmodulin studied by ^{15}N relaxation using inverse detected two-dimensional NMR spectroscopy: The central helix is flexible. *Biochemistry 31*, 5269−5278.

(8) Yuan, T., Ouyang, H., and Vogel, H. J. (1999) Surface exposure of the methionine side chains of calmodulin in solution. A nitroxide spin label and two-dimensional NMR study. *J. Biol. Chem. 274*, 8411−8420.

(9) Tjandra, N., Kuboniwa, H., Ren, H., and Bax, A. (1995) Rotational dynamics of calcium-free calmodulin studied by ^{15}N-NMR relaxation measurements. *Eur. J. Biochem. 230*, 1014−1024.

(10) Park, H. Y., Kim, S. A., Korlach, J., Rhoades, E., Kwok, L. W., Zipfel, W. R., Waxham, M. N., Webb, W. W., and Pollack, L. (2008) Conformational changes of calmodulin upon Ca^{2+} binding studied with a microfluidic mixer. *Proc. Natl. Acad. Sci. U.S.A. 105*, 542−547.

(11) Koch, M. H., Vachette, P., and Svergun, D. I. (2003) Small-angle scattering: A view on the properties, structures and structural changes of biological macromolecules in solution. *Q. Rev. Biophys. 36*, 147−227.

(12) Kaplan, J. H., and Ellis-Davies, G. C. (1988) Photolabile chelators for the rapid photorelease of divalent cations. *Proc. Natl. Acad. Sci. U.S.A. 85*, 6571−6575.

(13) Ellis-Davies, G. C., Kaplan, J. H., and Barsotti, R. J. (1996) Laser photolysis of caged calcium: Rates of calcium release by nitrophenyl-EGTA and DM-nitrophen. *Biophys. J. 70*, 1006−1016.

(14) Gill, S. C., and von Hippel, P. H. (1989) Calculation of protein extinction coefficients from amino acid sequence data. *Anal. Biochem. 182*, 319−326.

(15) Inoue, K., Oka, T., Suzuki, T., Yagi, N., Takeshita, K., Goto, S., and Ishikawa, T. (2001) Present status of high flux beamline (BL40XU) at SPring-8. *Nucl. Instrum. Methods Phys. Res., Sect. A 467*, 674−677.

(16) Huang, T. C., Toraya, H., Blanton, T. N., and Wu, Y. (1993) X-ray powder diffraction analysis of silver behenate, a possible low-angle diffraction standard. *J. Appl. Crystallogr. 26*, 180−184.

(17) Wakayama, J., Tamura, T., Yagi, N., and Iwamoto, H. (2004) Structural transients of contractile proteins upon sudden ATP liberation in skeletal muscle fibers. *Biophys. J. 87*, 430−441.

(18) Hammersley, A. P. (1997) FIT2D: An Introduction and Overview. ESRF Internal Report, ESRF97HA02T.

(19) Guinier, A., and Fournet, G. (1955) *Small-Angle X-ray Scattering*, John Wiely and Sons, New York.

(20) Svergun, D. I., and Koch, M. H. (2003) Small-angle scattering stuies of biological macromolecules in solution. *Rep. Prog. Phys. 66*, 1735−1782.

(21) Svergun, D. I., Barberato, C., and Koch, M. H. (1995) CRYSOL: A program to evaluate X-ray solution scattering of biological macromolecules from atomic coordinates. *J. Appl. Crystallogr. 28*, 768−773.

(22) Chattopadhyaya, R., Meador, W. E., Means, A. R., and Quiocho, F. A. (1992) Calmodulin structure refined at 1.7 Å resolution. *J. Mol. Biol. 228*, 1177−1192.

(23) Lewit-Bentley, A., and Rety, S. (2000) EF-hand calcium-binding proteins. *Curr. Opin. Struct. Biol. 10*, 637−643.

(24) Seaton, B. A., Head, J. F., Engelman, D. M., and Richards, F. M. (1985) Calcium-induced increase in the radius of gyration and maximum dimension of calmodulin measured by small angle X-ray scattering. *Biochemistry 24*, 6740−6743.

(25) Yoshino, H., Minari, O., Matsushima, N., Ueki, T., Miyake, Y., Matsuo, T., and Izumi, Y. (1989) Calcium-induced shape change of calmodulin with mastoparan studied by solution X-ray scattering. *J. Biol. Chem. 264*, 19706−19709.

(26) Kataoka, M., Persechini, A., Tokunaga, F., and Kretsinger, R. H. (1996) The linker of calmodulin lacking Glu84 is elongated in solution, although it is bent in the crystal. *Proteins 25*, 335−341.

(27) Ikura, M., Clore, G. M., Gronenborn, A. M., Zhu, G., Klee, C. B., and Bax, A. (1992) Solution structure of a calmodulin-target peptide complex by multidimensional NMR. *Science 256*, 632−638.

(28) Fallon, J. L., and Quiocho, F. A. (2003) A closed compact structure of native Ca^{2+}-calmodulin. *Structure 11*, 1303−1307.
(29) Wang, Q., Liang, K. C., Czader, A., Waxham, M. N., and Cheung, M. S. (2011) The effect of macromolecular crowding, ionic strength and calcium binding on calmodulin dynamics. *PLoS Comput. Biol. 7*, e1002114.
(30) Cheng, H., and Lederer, W. J. (2008) Calcium sparks. *Physiol. Rev. 88*, 1491−1545.
(31) Drum, C. L., Yan, S. Z., Bard, J., Shen, Y., Lu, D., Soelaiman, S., Grabarek, Z., Bohm, A., and Tang, W. J. (2002) Structural basis for the activation of anthrax adenylyl cyclase exotoxin by calmodulin. *Nature 415*, 396−402.